Projectile n distributions following charge transfer of Ar^+ and Na^+ in a Na Rydberg target

K. B. MacAdam, L. G. Gray, and R. G. Rolfes*
Department of Physics and Astronomy, University of Kentucky, Lexington, Kentucky 40506-0055
(Received 16 May 1990)

The n distributions produced by charge transfer of Ar^+ and Na^+ ions in a target of Na(nl) Rydberg atoms were extensively measured at intermediate velocities. The 60–2100-eV ions bombarded a laser-excited atomic-beam target. The projectiles were neutralized by capture into Rydberg states of Ar and Na and were analyzed by field ionization in an inhomogeneous-field detector whose response over states and energies was carefully mapped. The choice of initially prepared Na states, 24d, 25s, 28d, 29s, 33d, and 34s, allowed a comparison of $l=0$ and ≥ 2 targets at nearly equal binding energies over a range of reduced velocity $\bar{v}=0.187$ to 1.95. Capture populates m sublevels broadly, not merely $m \approx 0$. Overlapping contributions from adiabatic and diabatic modes of field ionization were accommodated in the analysis, which used a maximum-entropy-principle parametric form to fit the observed final-state distributions. The peak of the distributions, n_{max}, shifts upward from a value less than the initial state n_i to a value one to three units higher than n_i at $\bar{v}$ between 0.7 and 0.9 and ultimately shifts downward below n_i as $\bar{v}$ is further increased. The distributions become significantly sharper where the maximum upward shift occurs. Two ratios were defined to express the widths of final-state distributions in relative terms, one measuring the spread of orbital kinetic energy and the other the spread of Bohr-orbit velocity. By these ratios a universal behavior over energies, states, and projectile species is observed, and small differences between $l=0$ and ≥ 2 targets may be seen. A theoretical understanding of the present results, which span velocities where both molecular and perturbative theories are normally used, will require a quantal formulation that models the free-ranging response that is a hallmark of the high-quantum-number limit.

I. INTRODUCTION

Charge transfer in the collision at intermediate velocities between a singly charged ion and a highly excited Rydberg target atom presents an opportunity to study the dynamics of rearrangement in a quantal three-body system near the correspondence-principle limit. Hundreds of states of the target and projectile can participate in the interaction, and they have such a variety of angular momenta (l,m_l) and closely spaced energies that they should exhibit a free-ranging dynamic response that would be suppressed by the paucity and wide spacing of states at low n. In this paper we report extensive results of a new experiment[1] in charge transfer from laser-excited Rydberg atoms, and we reanalyze the complementary data of an earlier generation of the experiment.[2,3] Ar^+ and Na^+ projectiles at kinetic energies 60–2100 eV collide with Na(nl) in a crossed-beam geometry. These projectile energies span a range of reduced velocity $\bar{v}=v_{ion}/v_e$ from 0.2 to 2, where v_e is the root-mean-square orbital velocity of the Rydberg electron in the initial state of the target. [We take $v_e=(1/n_{eff})$ a.u., where the effective quantum number is $n_{eff}=n_i-\delta_l$.[4] n_i is the principal quantum number of the initial state. For a state with negligible quantum defect δ_l, v_e equals the orbital velocity of the nth Bohr orbit.] The projectile speed thus extends from a region where collisions may be described by a molecular model to a region where perturbative methods begin to become appropriate.[5] The relative distribution of excited states formed on the projectile, and the variation of this distribution with target state nl and velocity $\bar{v}$, are the chief objectives of this work. Target states 24d, 25s, 28d, 29s, 33d, and 34s are selected to span as large a range as practicable of binding energy, orbital velocity, and spatial extent. The optically accessible Na s and d states furthermore provide a contrast between targets of nearly pure $l=0$ character[6] and targets containing a diffuse mixture of low- or intermediate-l values resulting from l-change collisions in the target.[7,8]

A number of authors have addressed the matter of final-state distributions in electron capture, both theoretically and experimentally and over a wide range of velocities. Harel and Salin[9–11] and Janev and Winter[12] have discussed the physical mechanisms that influence final-state distributions in the context of capture by multiply charged ions. Capture preferentially populates excited states having $n \approx q^{3/4}$ for projectiles of charge state q,[13] and thus there may be a dense variety of available final states if q is sufficiently high.[14] Therefore many of the considerations in collisions of highly charged ions are relevant to the present work with Rydberg targets. For ground-state targets, however, target states remain sparse, and the initial state seldom has l higher than 0 or 1. Harel and Jouin[15] have recently discussed the energy dependence of subshell distributions and the influence of the atomic core by using a molecular expansion. Grozdanov and Belic[16] describe the rotational m mixing that follows capture at localized radial separations. Briggs[5] gives an overview of charge-transfer theories covering the

entire range from very slow to very fast collisions and emphasizing semiclassical conceptions of the process. Burgdörfer and Dubé[17] have described the broad, velocity-dependent final-state l distributions at intermediate and high velocity predicted by various theories of charge transfer, particularly by a modified continuum-distorted-wave treatment. Burgdörfer, Morgenstern, and Niehaus[18] have extended the classical over-barrier model for capture by slow highly charged ions to obtain final-l distributions. Jain, Lin, and Fritsch[19] have used an AO+ method to obtain complete density matrices for excitation and capture into $n=2$ and 3 of hydrogen in $p+\mathrm{H}(1s)$ collisions at intermediate velocity. For $v<0.57$ a.u. the captured electron resides in front of the projectile and for $v>0.77$ a.u. behind it. This is a change of dynamical behavior that occurs in a relative velocity range highlighted by the Rydberg results below. The classical-trajectory Monte Carlo (CTMC) method has been used by Olson and Isler[13,20] to calculate final n,l distributions following capture from $\mathrm{H}(n)$ by fully stripped ions. The CTMC with resolved initial l has been used by Becker and MacKellar[21] to calculate capture distributions at $\bar{v}=1-2$. Their final-n distributions agree well with current experimental results when the initial l is assumed small ($l=2$), but all-l or high-l initial distributions give markedly different results. MacKellar and Becker[22] find a very wide range of final-l and -m_l populations at $\bar{v}=1$ despite a narrow initial angular momentum distribution in a hydrogenic $28d$ state.

Brower and Pipkin[23] have measured the l and m_l distributions in $p+\mathrm{H}(1s)$ capture into $\mathrm{H}(n=3)$. Ashburn *et al.*[24] have measured density matrices for capture by protons in He into $\mathrm{H}(n=3)$. Vernhet *et al.*[25] have demonstrated by x-ray spectroscopy that capture by Al^{12+}, Al^{13+}, and Ne^{9+} ions at 4 keV/u populates excited states with mean n values 5–7 and mean l values 3–5. Müller *et al.*[26] describe a different approach from the present one to the detection and analysis of Rydberg ensembles obtained in experiments on dielectronic recombination. DePaola *et al.*[27] have described a measurement of final-n distributions in capture by fast highly charged ions. The experiment uses an alternate implementation of the inhomogeneous-field stripper analyzer described in Ref. 28.

The problem of capture by singly charged ions from a state-selected Rydberg target has a graphic appeal as a prototype three-body problem with equal forces in a region where all three particles have comparable speeds in their common center of mass. Despite the wide application of perturbative models much as the various forms of the Born approximation, such models become inapplicable for $\bar{v}<1$. The CTMC technique[13,20–22] does not describe important tunneling and interference behavior. Molecular-orbital treatments[12] have not been applied to these Rydberg collisions because they become impractical as $\bar{v}=1$ is approached from below, especially when the collision is not dominated by isolated pseudocrossings of a few potential curves.

Our past experimental work on charge transfer from Rydberg atoms[2,3,4,29] has demonstrated that capture proceeds to a range of final states with principal quantum numbers n approximately centered on n_i. The final-state n distributions broaden and shift downward in n as $\bar{v}$ is increased beyond 1. The narrowest distributions were those at the lowest reduced velocities investigated until now, about $\bar{v}=0.6$. No direct information about the final-l distribution has been obtained, but we expect no sharp selectivity in l. This follows because all but the lowest l states of projectile and target are nearly degenerate, and Stark mixing at small intermolecular distances R couples all l values strongly.[10] However, some evidence exists for a restriction on the change Δm_l of the projection of l along the direction of the incoming ion velocity.[10,11,29] (Hereafter, we designate m_l as m since spin plays no significant role in this work.) Nonetheless, as will be shown later, the experimental final-state distributions do not exhibit a concentration at low m values, and rotational mixing[10,11] occurring between the primary electron-transfer process at small R and the separation to $R=\infty$ should widely mix all values $|m|\leq l$. No other work has been reported on the distribution of final states in charge transfer from atomic targets prepared in selected Rydberg states.

Section II describes the experimental method. The final-state distributions are determined by use of a specially developed field-ionization detector,[28] whose properties and calibration must be carefully established. The new experimental data and data from the earlier (1982) experiment are summarized in Sec. III. Section IV describes the new method of data analysis based on overlapping contributions of field ionization from adjacent n manifolds[1] and the fitting of data to a parametric formula that is based on the maximum-entropy principle (MEP).[30] The results of this analysis are described in Sec. V, where two dimensionless ratios R_{KE} and R_{Bohr} are defined that illustrate the relative sharpness of electron velocity and kinetic energy in the capture distributions of projectile Rydberg states. The final-state distributions are seen to reach their minimum breadths and highest central n values near $\bar{v}=0.75$. In Sec. VI we discuss the results of the experiments in general terms and urge the development of new theoretical methods capable of handling strongly coupled quantal systems of very large numbers of states for this and other applications.

II. METHOD

A. Stripper-analyzer operation

The detector used in this work to determine the n distributions in Rydberg-state Ar or Na projectiles following charge transfer was described previously.[28] The detector consists of an inhomogeneous-field stripper constructed from coaxial half-cylinder electrodes, placed with their common axis perpendicular to the beam, and an electrostatic energy analyzer placed to receive projectiles that are field ionized during their passage between the cylinders. After leaving the interaction region where charge transfer occurs, the Ar or Na projectile beam passes between parallel plates (2 cm spacing by 6 cm

long) that apply a transverse electric field to sweep unneutralized Ar^+ or Na^+ ions out of the beam into an off-axis Faraday cup. Neutral projectiles in Rydberg states pass through a rectangular opening (7 mm wide by 10 mm high by 6 mm thick) in the stripper's outer cylinder, which is held at ground potential. The inner cylinder is set at a variable negative potential V_S up to -5000 V so that the projectiles, traveling along a radius between the cylinders, encounter an increasing electric field in the forward direction. The field $F(r)$ varies as $1/r$, where r is the distance from the axis of the cylinders. Biased guard plates are used to correct for truncation of the cylinders. When a given Rydberg-atom projectile reaches a sufficiently intense field to Stark ionize, the Ar^+ or Na^+ core is accelerated forward through the potential difference (which varies logarithmically with r) that remains before passing through a grid-covered aperture in the inner cylinder. (The liberated electron is accelerated backward and is not detected.) After a 7-cm drift the ion enters a 127° cylindrical analyzer whose slit and median-trajectory potentials equal V_S. A channel electron multiplier (CEM) in a shielded enclosure registers the arrival of individual ions at the exit slit.

Final-state distributions are recorded by scanning V_S in steps throughout the range -440 to -4600 V and accumulating CEM counts during a 10-μs gate that is delayed appropriately after each laser flash. Data are accumulated for fixed multiples of 256 laser flashes (at laser repetition rate 20 Hz) depending on the counting rates and statistics. For each primary-ion beam energy E the analyzer is tuned to focus ions that have gained $E_g = 200$ eV by acceleration in the stripper. The analyzer bandwidth has full width at half maximum of approximately $\Delta E = (E + E_g)/21$. As $|V_S|$ is increased, the equipotential surface that is 200 V more positive than the inner cylinder moves toward smaller r so that $F(r)$ increases correspondingly. Thus Rydberg atoms detected at larger stripper voltages $|V_S|$ are those that have field ionized in stronger fields. Generally speaking, they are those of lower principal quantum numbers n. The exact correspondence between n and the ionizing field depends on the details of field ionization and is addressed in Sec. IV. However, the one-to-one correspondence of F and V in this cylindrical geometry allows a sensitivity function to be measured directly as a function of V_S using accelerated Na(ns) Rydberg atoms that are injected directly into the stripper.[28] The measured sensitivities are associated with the charge-transfer signals in Ar or Na appearing at the same values of V_S.

The nonuniform sensitivity over the range $n \approx 20-50$ arises from the variations of ion trajectories in the inhomogeneous fields of the stripper. For electrostatic optics, the trajectories are a function of projectile kinetic energy and not separately of mass or velocity. For experiments at a given collision energy E the analyzer pass energy is fixed at $E + 200$ eV, and the entire analyzer is floated on V_S so that its properties do not vary as the stripper is tuned over the range of n. Likewise the impact energy of ions in the CEM cone is constant over the tuning range of the stripper at each E.

B. Detector sensitivity calibration

Auxiliary measurements were made by the method described in Ref. 28 to calibrate the V_S- and E-dependent sensitivity of the detector. In brief, Na^+ from a Colutron ion source was accelerated to each desired E, neutralized in a Na vapor cell, and laser excited in the interaction region to ns states, $n = 21-38$, used as markers. Each Na(ns) marker state, upon entering the stripper analyzer, gave rise to a peak in the detector response over a small range of V_S, typically 160 V. The area of this peak was normalized by the average Na^0 flux and by the number of Na(ns) atoms excited in the thermal atomic beam at the interaction region at the same time. Corrections for detector pileup and radiative decay[31] during the flight between the interaction region and the detector were applied. Although counting rates in the calibration runs were very low (0.02 to 0.3 counts per laser flash) there was no measurable background within the 500-ns CEM counting windows that were delayed after the laser shots according to the Na time of flight. Detector sensitivity was measured over the range $V_S = -600$ V ($n = 38$) to -4660 V ($n = 21$) at several energies E between 270 and 2100 eV. [In 1982, calibrations of the same detector were obtained for $n = 23-38$ at energies 750–2000 eV. However, the calibration extended only to $V_S = -3180$ V, and no lifetime corrections for Na(ns) states were applied.] Figure 1 shows typical sets of calibration points. Particularly at the lower energies, $E < 1000$ eV, and higher stripper voltages, $|V_S| > 3000$ V ($n = 21-23$), a significant

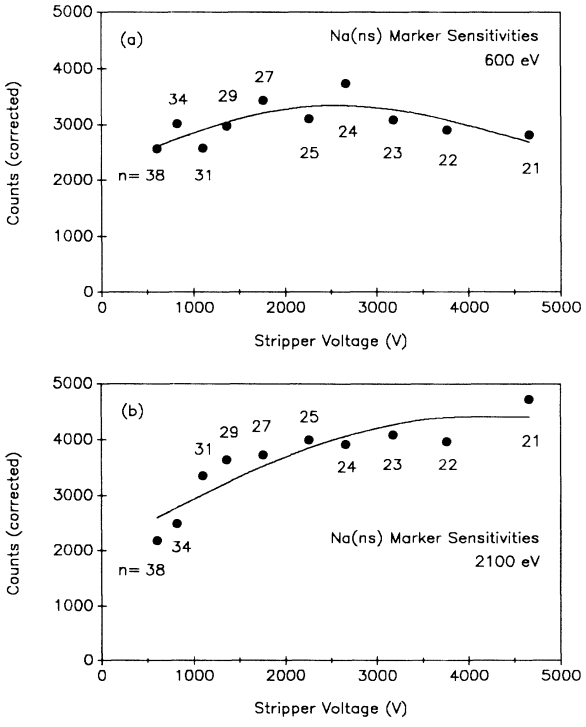

FIG. 1. Variation of detector sensitivity with n and projectile kinetic energy: (a) 600 eV; (b) 2100 eV. The smooth curves are least-squares fits using Eq. (1).

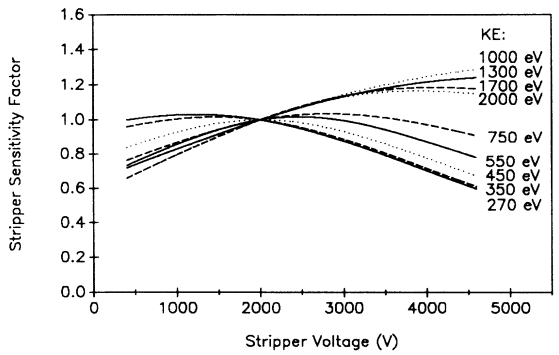

FIG. 2. Detector sensitivity function Eq. (1) as fitted to Na(ns) marker calibrations between 270 and 2100 eV.

curvature in the sensitivity over V_S is evident. (The 1982 calibrations were consistent with the present ones, but no curvature was conclusive in the more limited range of calibration data. A linear and energy-independent sensitivity function was thus assumed in the 1982 analysis of data.[2,3] The older charge-transfer data will be reanalyzed below based upon the new calibrations.) To aid interpolation each set of calibration points was fitted by a smooth empirically based curve. We write

$$f(x)=C\frac{1+A_1(x-2000)}{1+A_2(x-2000)^2} \quad (1)$$

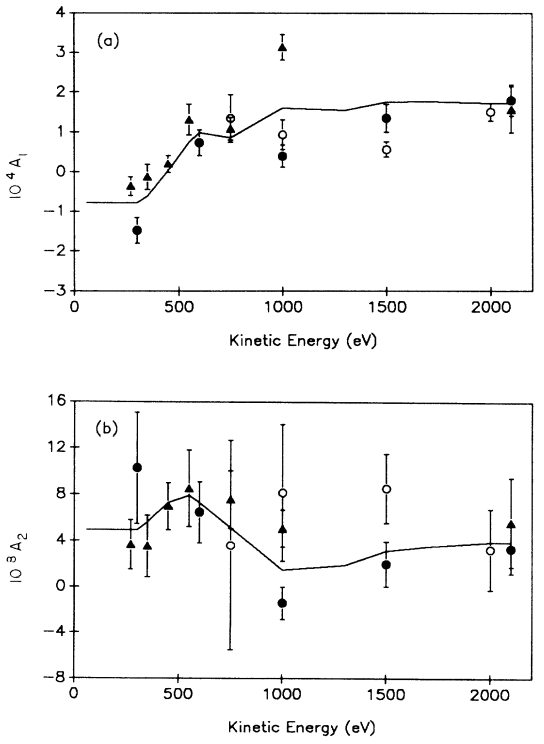

FIG. 3. (a) Linear detector sensitivity coefficient A_1, Eq. (1); (b) quadratic coefficient A_2. Solid circles and triangles, 1989 data; open circles, 1982 data; line, weighted interpolation of 1989 calibration points.

where $x=|V_S|$ in volts. Figure 2 shows the resulting sensitivity functions, normalized to one at 2000 V. A consistent pattern of sensitivity variation is apparent. It was unfortunately not possible to obtain detector calibrations at $E<270$ eV because of declining Na neutral beam intensity, counting rates, and apparatus stability. Although charge-transfer experiments were run at energies as low as 60 eV by mounting the ion source only 15 cm from the interaction region, there was not enough room then to introduce the necessary vapor cell, cleanup deflectors, and beam dump between the source and the interaction region to make the corresponding sensitivity calibrations. Figure 3 shows the variation of calibration constants A_1 and A_2 with E and indicates the extrapolated values on which charge-transfer data analysis at $60\leq E\leq 205$ eV was based.

C. Adiabatic and diabatic field ionization in the stripper

Many earlier works have demonstrated the occurrence of two categories of selective field ionization (SFI) in Na Rydberg states, termed adiabatic (ASFI) and diabatic (DSFI).[32,33] ASFI refers to the ionization of Stark levels when, in an increasing field F, they cross and mix strongly with more rapidly ionizing levels that arise from higher n values.[34,35] In Na, Stark levels having $|m|=0$, 1, and 2 are generally subject to ASFI because the corresponding quantum defects δ_s, δ_p, and δ_d are large enough to couple hydrogenic states of differing n manifolds.[36] For $|m|\geq 3$, and also for $|m|=2$ when $n\geq 32$, the intermanifold couplings at avoided crossings are so weak that n sublevels are carried to higher F without field ionizing adiabatically. At fields two to four times those characteristic of ASFI the higher-$|m|$ sublevels ionize by the hydrogenic tunneling mechanism in DSFI.[32] Intermanifold avoided crossings are breached diabatically. Quantum defects in Ar are larger than those in Na, but the same general SFI behavior is expected to occur.[3] The transition between ASFI and DSFI in Ar would be shifted upward by perhaps one $|m|$ value relative to Na.

The result is that the ionization occurring at a field F or stripper voltage V_S in the detector cannot uniquely be assigned to a principal quantum number n since the ASFI and DSFI signals of nearby n's overlap. In our earlier work[2] it was assumed, and a justification was offered, that Rydberg states entering the detector were primarily in low-$|m|$ sublevels and consequently underwent ASFI. It is a property of ASFI that the field ranges for ionization of all the sublevels of a given n do not overlap with those of adjacent n's.[35] Therefore it was possible to establish a point-for-point correspondence between ionizing field F and the n quantum number, which was taken as a continuous parameter, the Stark principal quantum number n_S. The resulting relationship was in close agreement with the widely applicable $1/n^4$ variation of fields necessary to achieve field ionization. In our earlier work[2] we took $F=Cn_S^{-\beta}$, where $C=(2.915\pm0.008)\times10^8$ V/cm and $\beta=3.925\pm0.016$, as derived from the measured positions of the Na(ns) marker peaks, for which we assigned $n_S=n-1.5$

New measurements have indicated that the distribution of $|m|$ values of Rydberg atoms entering the stripper is not concentrated at the lower values that would undergo ASFI. For example, charge-transfer products in a test case $Na^+(1000\ eV)+Na(28d)$ were exposed to transverse and longitudinal magnetic fields in the 23-cm drift space between the interaction region and the stripper. A transverse field $B_\perp \approx 2.5$ G would cause the precession of orbital magnetic moments at the Larmor frequency from directions primarily perpendicular to the ion beam (low $|m|$ along the beam direction) into the beam direction (high $|m|$) and would change the ASFI behavior to DSFI. However, no statistically significant change in the variation of stripper count rate over the range of V_S was observed when such a field was applied. An alternative explanation of this null result, if the capture process itself populated mainly low-$|m|$ sublevels, is that the distribution might become broadened over the entire range of $|m|$ by random precession in small stray magnetic fields normally encountered in the drift space. To weigh this scenario, a longitudinal magnetic field $B_\parallel = 32$ G was applied in the same test case to lock the orbital moments onto a dominant axial field that would preserve $|m|$. Again no difference from the normal $B=0$ charge-transfer distribution was seen. We conclude that the distribution of manifold states entering the detector is intrinsically broad in $|m|$ along the beam direction so that its redistribution by $B_\perp$ causes no net change of the $|m|$ populations. It is still possible that some intense (although unknown and unobserved) perturbation causes diffusion of an intrinsically narrow $|m|$ distribution that is formed initially in the charge-transfer process. But it must be much more effective than the applied longitudinal field to account for the lack of an observable effect in the $B_\parallel$ test. If the primary electron-transfer process occurs when the internuclear axis is substantially transverse, a population restricted by a $\Delta m = 0$ rule along this axis would transform to a broad m distribution along the beam direction since the electronic wave function would not follow the axis rotation adiabatically.[11,37] l and m mixing of Rydberg atoms from other charged projectiles in the beam is another possible explanation.[7,37] Finally, if only s, p, and d states of the projectile were populated by charge transfer, precession of magnetic moments by the transverse field would *not* result in a significant amount of DSFI. However, such an l selectivity seems unlikely[11,12] and would cause observable undulations in the stripper distributions, which are not in fact present. In any event, whether from the ion-atom collision itself or from external or subsequent influences, the $|m|$ distribution of Rydberg atoms that enter the stripper exhibits the SFI characteristics of a uniform population of Stark sublevels in each n manifold. This means that the analysis of charge-transfer data and the inference of distributions over n must take account of the overlapping signals, including both ASFI and DSFI, at every stripper voltage. It is not then possible to make a point-for-point correspondence between F and n_S as was formerly done. Section IV B below describes the method of data analysis based on overlapping SFI contributions.

SFI patterns in the detector similar to those that would be obtained from uniform sublevel distributions in single n manifolds are shown in Fig. 4. Accelerated Na^0 atoms, as used in the sensitivity calibrations, were excited to $n=24$, 28, and 33 in the presence of a small electric field perpendicular to the beam axis. The 410-nm laser was tuned so that its 1-cm^{-1} linewidth excited many Stark-mixed states in the middle of the manifold. The laser line was narrow enough that no sublevels of adjacent n values were excited. The polarization of the laser was parallel to the mixing field so that predominantly $|m|=0$ and 1 sublevels were excited relative to the axis of the mixing field.[38] The electric field in the stripper was, however, parallel to the ion-beam direction, so with respect to the (rotated) quantization axis appropriate to SFI in the stripper the laser-excited population contained a broad range of all $|m|$ up to the maximum value $n-1$.[37] To homogenize the manifold distribution further, a transverse magnetic field was applied to precess the magnetic

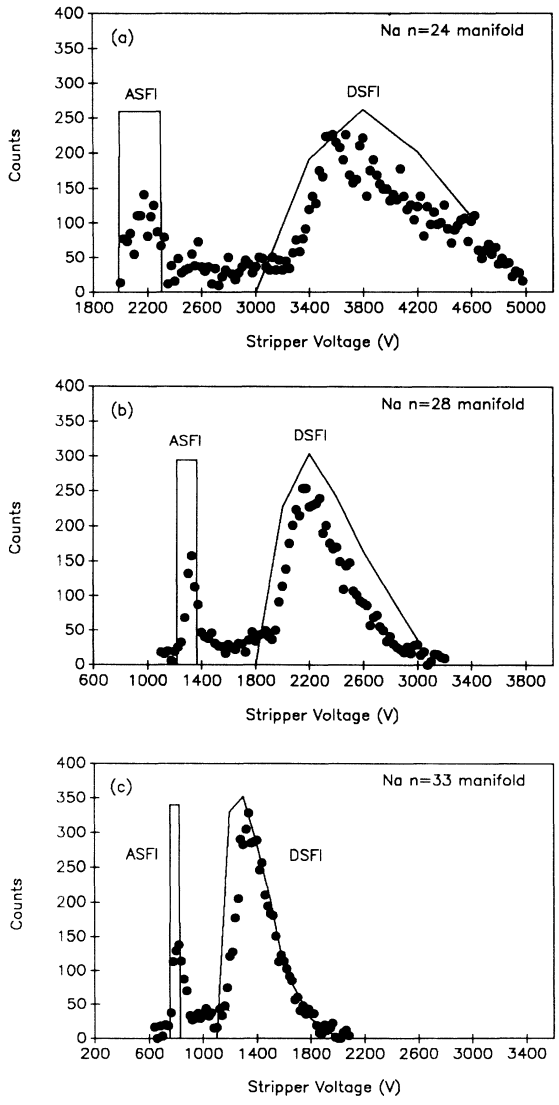

FIG. 4. Pseudo-full-manifold detector signals (see text). Dots, experiment; lines, numerically synthesized SFI signals. (a) $n=24$; (b) $n=28$; (c) $n=33$.

moments. The experimental signals (Fig. 4) exhibited a narrow peak positioned just where the ASFI for selectively excited states of that n occurred and a broad DSFI peak at roughly twice the ASFI field value. As described in Sec. IV B and shown in Fig. 4, these auxiliary signals corroborate the numerically synthesized detector signals that are used below for the analysis of overlapping n contributions.

It was possible in some cases to operate the apparatus in the mode used for selective excitation of fast vapor-cell-neutralized Na without any deflection plates or aperture between the interaction region and the stripper. We found (Fig. 5) that the effect of a deflection field (normally used to prevent unneutralized projectiles from entering the stripper) and a 6.4-mm postinteraction aperture was to extend and enhance the diabatic part of the SFI signal arising from $|m|=2$ sublevels of the Na($33d$) state. The change of DSFI shape in this case corresponded to the increased presence of $|m|\geq 2$ states throughout the $n=33$ manifold, not just at the lowest part that arose out of $l=2$. Such a manifold-homogenizing influence of the deflector and aperture, which were required for all charge-transfer runs, strengthens the conclusion that a broad or uniform distribution of sublevels throughout each m manifold should be assumed in the analysis of charge-transfer data.

The cross sections for l change of Na(nd) under Ar^+ or Na^+ bombardment are 2 or 3 orders of magnitude larger than for charge transfer.[7] Thus the laser-excited target of Na(nd) states is unavoidably l mixed by multiple collisions during charge-transfer measurements.[8,37] The targets designated "nd" are thus in fact targets exhibiting a range of low- and medium-l values of the same n. On the other hand, very little l change occurred with Na(ns) charge-transfer targets.[6] Comparisons made between ns and nd targets therefore probe differences in the charge-transfer process between pure $l=0$ and mixed $l\geq 2$.

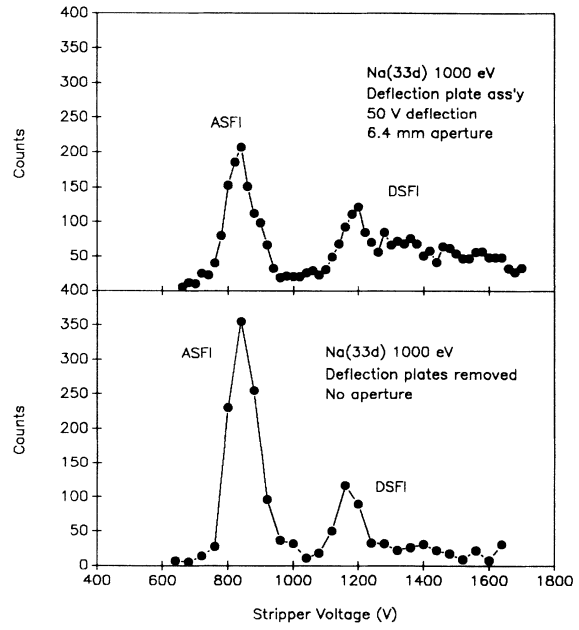

FIG. 5. Effect of deflection field and aperture on Na($33d$) detector signal at 1000 eV.

To test whether n change or l change occurred by collisions with background gas while charge-transfer products passed between the interaction region and the detector, tests were made allowing N_2, CO_2, or Ar gas into the beam line at pressures up to 1×10^{-5} torr. No change in the stripper distributions for selectivity excited Na(nd) at $E=500$, 1000, or 1500 eV was seen. This null result translates into an upper limit $\sigma<6\times10^{-12}$ cm^2 on the cross section for n and l change in fast collisions with these neutral targets assuming sensitivity at the 10% level to redistributions in the final-state populations that change the overall field-ionization profile.

III. EXPERIMENTAL DATA

A. Synopsis of new data

Charge transfer was studied for $Ar^+ + Na(nl)$ collisions at 14 energies between 60 and 2100 eV for 24d, 28d, and 33d targets. In addition, 25s, 29s, and 34s targets were used at 12 of the same energies $E\geq 115$ eV. (These s states were chosen because they have binding energies nearest to the chosen d states.) The reduced velocities covered by the new data ranged from $\tilde{v}=0.187$ to 1.518. Each scan of the final-state distribution took about one to two hours of uninterrupted running time. Two or three runs with each target state and energy were combined from separate days' operation to check consistency and to average out variations. The lower-energy limit was imposed by obtainable ion-beam currents. Typically 35 nA through a 9.5-mm-diam postinteraction aperture was required at the lowest energies for adequate counting rates, which were as low as 0.05 counts per laser shot in an appropriately delayed counting window. As described above, it was not possible to calibrate the n-dependent sensitivity of the detector below 270 eV, and efforts to reduce the energy range of charge-transfer measurements below 60 eV were therefore not taken. The high-energy limit was imposed by the requirement that the deflection field used to prevent unneutralized projectile ions from entering the stripper must not field ionize the highest-n Rydberg states registered by the detector ($V_S=-440$ V, $n\approx 56$ ASFI). The limiting value $F_{\text{deflector}}\leq 50$ V/cm provided adequate background reduction only for beam energies $E\leq 2100$ eV. A smaller 3.2-mm postinteraction aperture aided in background suppression for $E\geq 1300$ eV, and a 6.4-mm aperture was used at intermediate energies.

The background of counts not related to Rydberg charge-transfer products was normally insignificant. In one circumstance background subtraction was required, near $|V_S|=(E+E_g)/e$. In this case, projectile ions that reflected with small kinetic energy from surfaces at ground potential could find their way through the analyzer into the CEM because the analyzer slit bias accelerated them to the analyzer design energy.

B. Synopsis of 1982 data

Similar charge-transfer experiments[2,3] completed in 1982 provided data in overlapping ranges of energy and reduced velocity that will be reanalyzed below using the new detector calibrations. The case $Ar^+ + Na(25s)$ was studied at 33 closely spaced energies between 580 and 2000 eV, spanning the range $0.572 \leq \bar{v} \leq 1.062$. $Na^+ + Na(25s)$ was also studied at ten energies between 750 and 2000 eV ($\bar{v} = 0.858 - 1.400$). Charge transfer of $Na^+ + Na(nl)$ for $24d$, $28d$, $29s$, $33d$ and $34s$ was recorded between 550 and 2000 eV (except at 550 eV only the $33d$ and $34s$), thus reaching $\bar{v} = 1.95$. Nine other cases of $Ar^+ + Na(nl)$ for s and d states at $\bar{v} = 0.75$ and 1.00 were also measured.[4] It will be seen below that the reanalysis of 1982 data extends and illuminates the new results.

IV. ANALYSIS OF CHARGE-TRANSFER DATA

A. Maximum-entropy distribution

Extensive experimental study of final-n distributions in charge transfer from $Na(nl)$ Rydberg targets by Ar^+ and Na^+ projectiles[2,3] has shown that there is no detectable structure, i.e., rapid variation of counting rates as a function of ionizing electric field, within a single broad maximum. Only variations of peak position, width, and upper or lower inflection points are apparent. The n distributions should therefore be describable empirically by a small number of parameters. For such a description the recently obtained[30] maximum-entropy-principle (MEP) distributions have been found satisfactory and will be used to obtain a comprehensive representation of the widely varying experimental data.

The MEP final-state distribution is given by

$$P(n) = Cf(n)\exp[-\lambda(1/n - 1/n^*)^2] \tag{2}$$

where $P(n)$ is the number of atoms having principal quantum number n, C is a normalization constant, $f(n)$ is a "prior" distribution or statistical weight, λ controls the width of the distribution, and n^* controls its center. Three reasonable choices of $f(n)$ are (i) $f(n) = n^2$, corresponding to the case where all final (l,m) substrates are equally populated for each n; (ii) $f(n) = n$, corresponding to the case where m takes only a fixed range of values, e.g., $m \approx 0$; and (iii) $f(n) = 1$, corresponding to the case where both l and m are restricted to a limited number of values. In previous fitting of Rydberg charge-transfer data by (2) the three choices fitted almost equally well with $f(n) = 1$ best by a slight margin.[30] Since it was formerly assumed[2,3] that only low-m values were populated by charge transfer (and possibly only low l also), $f(n) = 1$ seemed to be the logical, as well as the best-fitting, choice.

Based upon the magnetic-field tests and other comments above, we now believe that a wide, possibly complete range of l and m values is present for each n in the final-state distribution. However, we believe on theoretical grounds that an m selection rule operates in the primary transfer process itself and that the rotation of the internuclear axis toward the direction of the departing projectile is responsible for the mixing of m's. Thus n^2 final sublevels of manifold n (ignoring spin) are populated nearly uniformly, but the statistical weight of manifold n in the collisional transition is limited by a $\Delta m \approx 0$ preference to a value proportional to n. The rotational mixing[10,11] then serves merely to spread a given population formed in the primary transfer process among a larger number of sublevels. Therefore we chose $f(n) = n$ in (2) as the statistical weight of the n manifold,[39] but it will be assumed that each sublevel (l,m) is equally populated for a given n, that ASFI occurs for $|m| = 0$, 1, and 2, and that DSFI occurs for $3 \leq |m| \leq n - 1$.

B. Stripper-signal fits

Because the sublevels of adjacent n's ionize by DSFI at fields that overlap, the experimental counting rates cannot be converted from functions of V_S to functions of an equivalent n_S by a one-to-one relationship. Instead, the MEP parameters are inferred from the data as follows. For each n an equal-area detector signal is synthesized numerically by modeling the field ionization of a uniform (l,m) distribution entering the detector. $P(n)$ is used to assign a population to each n state for trial values of the MEP parameters, and the overall detector signal is then calculated by summation over n as a function of V_S. The calculated signal is compared with the experimental distribution over the range of V_S, and the MEP parameters are found by a Poisson-weighted multivariate least-squares procedure.[40] In what follows, this is referred to as a "stripper-signal fit."

The diabatic contribution ($m \geq 3$) to each synthesized detector signal was calculated by a method similar to that described by Kellert *et al.*[41] and MacAdam *et al.*[8] based on the hydrogenic ionization rates for parabolic states (n,n_1,m) (Ref. 42) except that the variation of electric field with time actually encountered by a projectile Rydberg atom inside the cylindrical stripper[28] was used. For each value $|V_S|$ within the experimental range, a fixed initial number of Rydberg projectiles was assumed to enter the field at velocity v_{ion}. The number of decays occurring by DSFI in successive increments of time was then calculated. The undecayed population advanced to a new radial position and encountered a stronger field F at a new potential V. The decay constant for each sublevel was recalculated, and the number of decays of the remaining population in the next time increment was found. In each step, the number of decays was associated with the increment of potential V encountered in that step because that potential determines the subsequent energy gain of the ions accelerated in the inhomogeneous field. When an electrostatic potential $V = V_S + 200$ V was encountered the number of decays occurring *per unit potential* V was taken as the signal at that stripper voltage V_S. This measure of the signal is appropriate for the mode of detector operation described above and corresponds to the constant energy resolution of the 127° analyzer over the tuning range of V_S for a given incident beam energy. Calculations required at each F the energies of all (doubly degenerate) Stark sublevels $|m| \geq 3$ subject to DSFI, $(n^2 - 5n + 6)/2$ energies in all. Energies were calculated by sixth-order perturbation theory.[43] The semiempirical

formula of Damburg and Kolosov[42] was used to find each corresponding decay rate. Faster projectiles penetrate farther into the inhomogeneous field before decaying, but calculations showed that the corresponding shift of the DSFI signal was less than one V_S step, e.g., a 30-V shift for $n=28$ DSFI over the argon kinetic-energy range 200–2000 eV. Subsequent calculations were made only for the 3.8×10^6 cm/s velocity of 300-eV Ar.

The synthesized DSFI signals were augmented by empirically based estimates of ASFI for the $|m|\leq2$ sublevels. The sublevels of each n manifold that undergo ASFI do so in nonoverlapping ranges of fields.[35] The correspondence between ionizing field F, stripper voltage V_S, and the Stark quantum number n_S was that used previously[2] for the all-ASFI analysis of Rydberg charge transfer. The final normalized estimate of the detector signal for a uniform distribution of (l,m) sublevels for a given n was found by adding a flat contribution for ASFI over the corresponding V_S range (with area given the statistical weight $5n-6$ of $|m|\leq2$ sublevels) to the calculated DSFI pattern (given statistical weight n^2-5n+6). The resulting profile normalized to unit area represented unit contribution of principle quantum number n to the final charge-transfer signal. Figures 4(a)–4(c) show examples of the calculated profiles for $n=24$, 28, and 33 and a comparison with homogenized experimental signals from the same manifolds.

Least-squares fitting of the MEP parameters by comparison of the $P(n)$-weighted synthesized detector profile with the experimental data showed a strong correlation between inferred values of λ and n^*. [Note that n^* identifies the peak $n_{\max}$ of $P(n)$ only for the case $f(n)=1$, but the preferred prior distribution $f(n)=n$ skews the exponential form so that the peak lies about one unit above n^*.] A redefinition of parameters in the MEP distribution,

$$P(n)=Cf(n)\exp\{-\mu[(n^*/n)-1]^2\} \tag{3}$$

where $\mu\equiv\lambda/n^{*2}$, served to remove most of this built-in correlation. μ, like λ, controls the width (or more accurately, the sharpness) of $P(n)$.

C. SFI centroid fits

An alternate but less satisfactory method of fitting $P(n)$ to the data was formulated with the advantage that experimental data and fits could be compared on a scale of n. The centroid field F_{cent} of each synthesized SFI profile for level n (including both ASFI and DSFI) was determined, and the resulting values were used to establish an n scale, i.e., a relationship between n and F or n and V_S. The centroid fields for ionization were fitted by the expression

$$F(\text{V/cm})=(3.3601\times10^8\ \text{V/cm})n^{-3.8096}. \tag{4}$$

This relationship was used to convert all experimental data to effective distributions over n, allowing for the compression of detector counts from successive n's into decreasing F or V_S ranges as n increases.[2,28] Fits of the resulting data to $P(n)$ with n treated as a continuous parameter, referred to as "SFI centroid fits," gave MEP parameters that were similar to those from the stripper-signal fits. But the wide dispersal and overlapping of signal contributions for adjacent n's makes it difficult to assess systematic modeling errors in the centroid fitting procedure. In a few cases [Ar^+ at 115, 155, 270, and 450 eV incident on Na(24d)], the centroid fit converged but the stripper fit did not. Nonetheless, the parameter values returned by the centroid fit in these cases were suspect on close examination. In several other cases, most of the 24d and 25s targets for $E\leq450$ eV, neither fitting procedure converged. When both procedures gave meaningful MEP parameter values, the n^* values agreed within their error bars. μ values differed by two to six times the combined errors, with smaller μ values for centroid fits. Owing to the crudeness of the SFI centroid fit method, its chief utility is to display experimental data and the MEP curve on a common scale of principal quantum number to aid in visualization. The stripper-signal fit is offered here as the correct way to extract MEP parameters from the data, and it would be used in case any other form of $P(n)$ were to be tested. Histograms of $P(n)$ with the parameter values determined in stripper-signal fits give a visual impression of the n distribution, but a direct comparison of data and fit must be made on the less easily interpreted scale of stripper voltage V_S.

V. RESULTS

Figure 6 shows the final-state distribution for Ar^+ (350 eV)+Na(28d). In Fig. 6(a) the accumulated detector counts, corrected for sensitivity variations, are plotted as a function of $|V_S|$. (The graph is normalized to a peak value 1000 for convenience.) The piecewise linear function represents the stripper-signal fit to this data. Figure 6(b) shows the same data set, adjusted to represent counts per unit Stark principal quantum number n_S, and the SFI centroid fit. Figure 6(c) shows $P(n)$ histograms for integer values $n=19-53$, using the optimized parameters of the stripper and centroid fits for comparison.

Figure 7 demonstrates $P(n)$ histograms based on stripper-signal fits of Ar^++Na(25s) at 350, 1000, and 2100 eV. Figure 8 shows the variation with $\bar{v}$ of the peak positions $n_{\max}$ of fitted final-state distributions. The reanalysis of 1982 data shown in Figs. 8(b) and 8(c) confirms and augments the new data of Fig. 8(a). The figures show that for slow collisions $\bar{v}<0.5$ and again for fast collisions $\bar{v}>1.5$, $n_{\max}$ lies below the principal quantum number of the target state by one to two units. However, all target states show an upward shift of the final-state distribution at intermediate velocities to values $n_{\max}$ that are one to three units *higher* than the initial n, the maximum upward shift occurring between $\bar{v}=0.7$ and 0.9.[9]

The MEP width parameter μ shows a very interesting behavior as a function of $\bar{v}$ [Fig. 9(a)]. For slow collisions, $\mu=12\pm2$. But μ rises to a fairly distinct maximum as high as 18 near $\bar{v}=0.7$, falling again before $\bar{v}=1.0$ to about $\mu=12$ and slowly declining afterward. Thus the distributions show a definite narrowing near the energy corresponding to projectile motion at about 0.7

times the orbital velocity. Again the 1982 data in Figs. 9(b) and 9(c) complement the picture offered by the new experiment.

In order to display physically suggestive measures of final-state widths, we define two semiclassically based quantities, the kinetic-energy ratio R_{KE} and the Bohr-velocity ratio R_{Bohr}, as follows (atomic units):

$$\sigma_{\mathrm{KE}}=\langle(1/2n^2-\langle 1/2n^2\rangle)^2\rangle^{1/2}\ , \tag{5}$$

$$(E_k^{\mathrm{rel}})_{\mathrm{rms}}=1/2n_{\mathrm{eff}}^2+v_{\mathrm{ion}}^2/2=(1+\tilde{v}^2)/2n_{\mathrm{eff}}^2\ , \tag{6}$$

$$R_{\mathrm{KE}}=\sigma_{\mathrm{KE}}/(E_k^{\mathrm{rel}})_{\mathrm{rms}}\ , \tag{7}$$

$$\sigma_{\mathrm{Bohr}}=\langle(1/n-\langle 1/n\rangle)^2\rangle^{1/2}\ , \tag{8}$$

$$(v^{\mathrm{rel}})_{\mathrm{rms}}=[2(E_k^{\mathrm{rel}})_{\mathrm{rms}}]^{1/2}=(1+\tilde{v}^2)^{1/2}/n_{\mathrm{eff}}\ , \tag{9}$$

$$R_{\mathrm{Bohr}}=\sigma_{\mathrm{Bohr}}/(v^{\mathrm{rel}})_{\mathrm{rms}}\ . \tag{10}$$

The velocity $(v^{\mathrm{rel}})_{\mathrm{rms}}$ is the root-mean-square speed of the Rydberg electron on the Na target before capture relative to the approaching projectile ion. It contains a contribution both from orbital motion in the target atom and from the projectile velocity in the laboratory frame. σ_{KE} is the rms deviation of electron orbital kinetic energy in the final-state distribution about the mean kinetic energy of the distribution. R_{KE} expresses the final kinetic-energy (KE) spread of the electron after capture as a fraction of its initial KE in the projectile frame. σ_{Bohr} is the spread of Bohr velocities $1/n$ a.u. in the final-state distribution about the mean. The ratio R_{Bohr} expresses the width of the velocity distribution of the active electron in terms of its initial velocity relative to the approaching ion. The ratios R_{KE} and R_{Bohr} are expressible in terms of moments $m_s=\langle(n_{\mathrm{eff}}/n)^s\rangle$, for $s=1$, 2, and 4, of the MEP final-state distributions[30] about the initial $n_{\mathrm{eff}}=n_i-\delta_l$ of

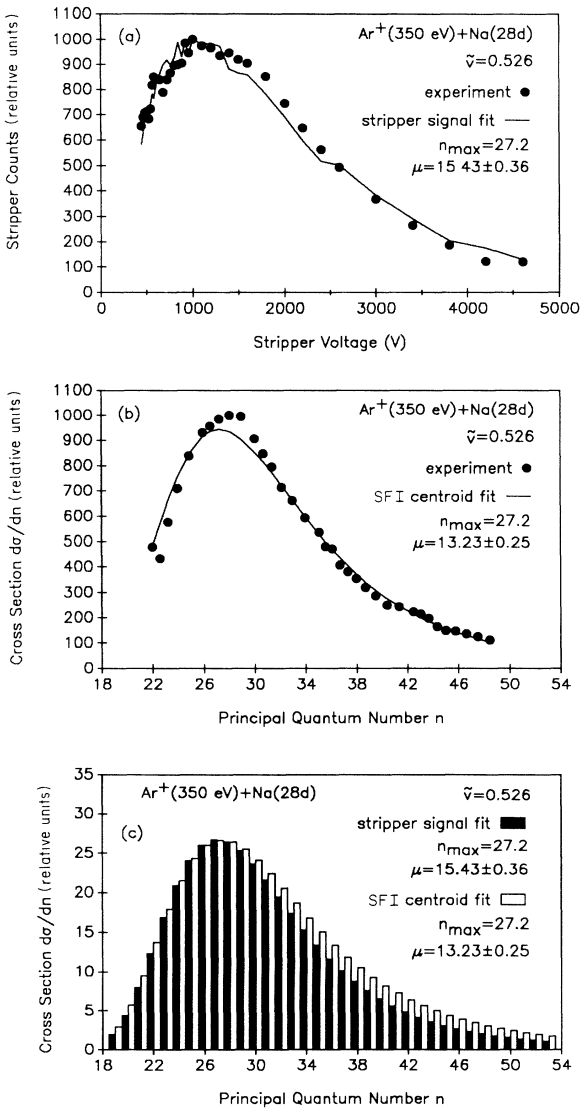

FIG. 6. Charge-transfer final-state distributions, $Ar^+(350\ eV)+Na(28d)$: (a) stripper signal and fit; (b) SFI centroid fit; (c) MEP distributions derived from (a) and (b).

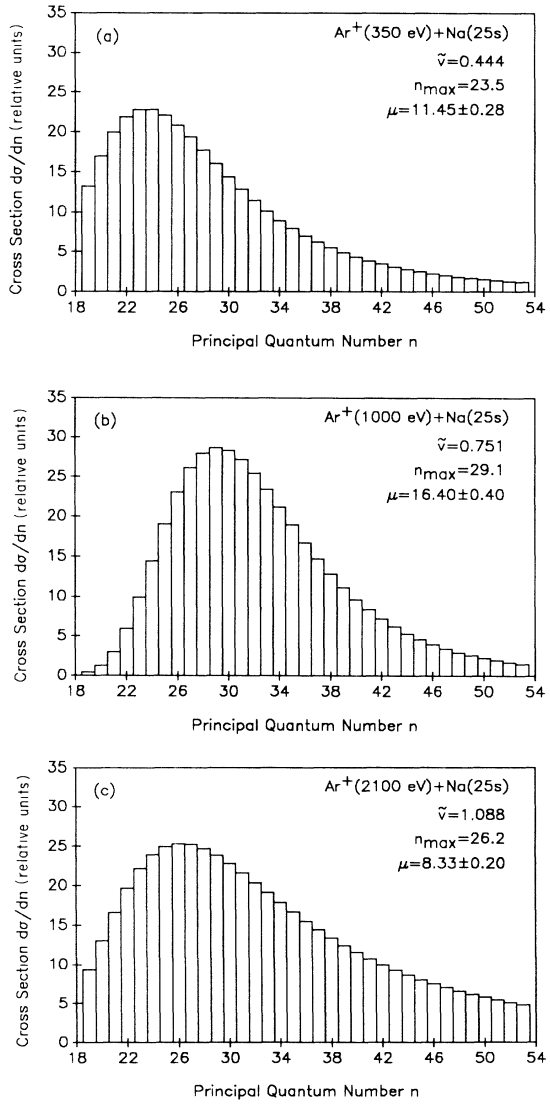

FIG. 7. Final-state histograms (MEP fits), $Ar^+ + Na(25s)$, demonstrating low-, intermediate-, and high-energy behavior. (a) 350 eV; (b) 1000 eV; (c) 2100 eV.

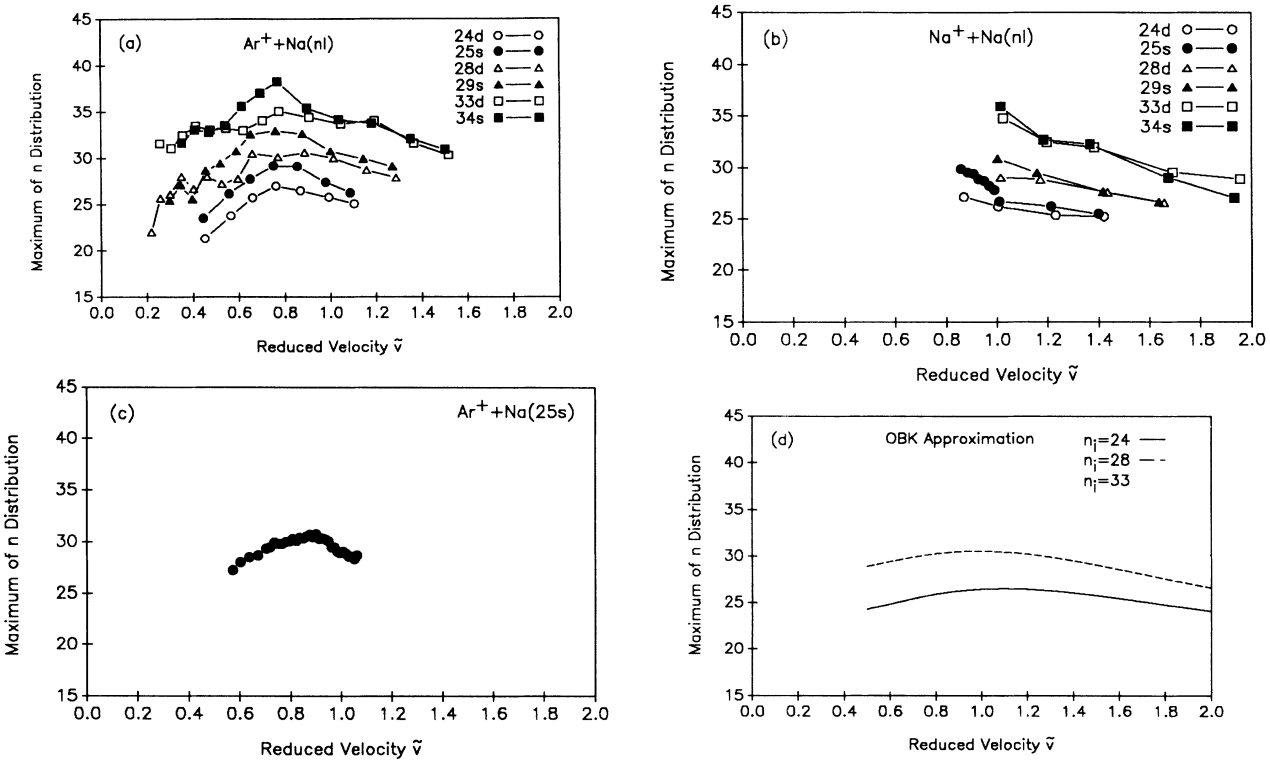

FIG. 8. Peak n value, n_{max}, of final-state distributions (stripper-signal fits). (a) New $Ar^+ + Na(nl)$ data; (b) 1982 data, $Na^+ + Na(nl)$; (c) 1982 data, $Ar^+ + Na(25s)$ only; (d) OBK approximation, Eq. (13) fitted by MEP, Eq. (3).

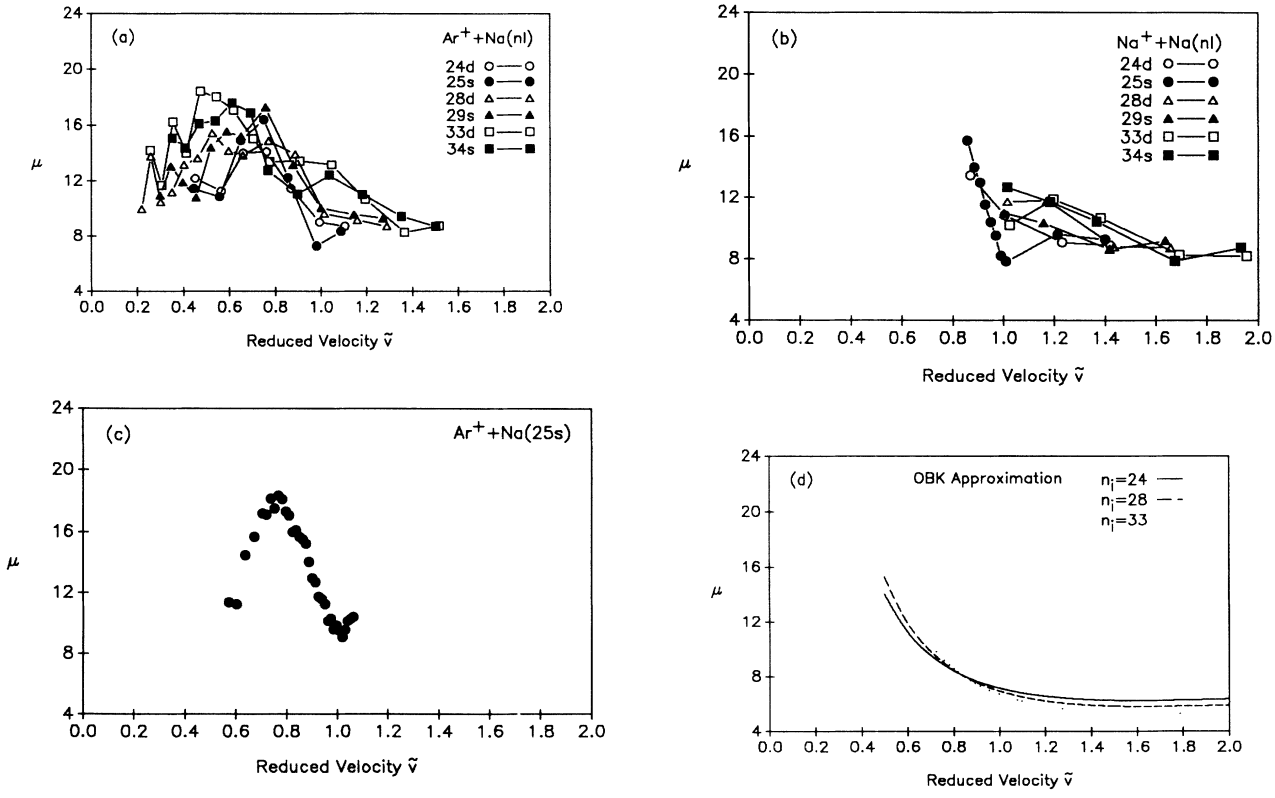

FIG. 9. Sharpness (width) parameter μ of MEP final-state distributions, obtained from stripper-signal fits. (a) New $Ar^+ + Na(nl)$ data; (c) $Na^+ + Na(nl)$, 1982; (c) $Ar^+ + Na(25s)$ only, 1982; (d) OBK approximation, Eq. (13) fitted by MEP, Eq. (3).

the target state[44] with quantum defect δ_l,

$$R_{\mathrm{KE}}=[(m_4-m_2^2)]^{1/2}/(1+\bar{v}^2)\ , \tag{11}$$

$$R_{\mathrm{Bohr}}=[(m_2-m_1^2)/(1+\bar{v}^2)]^{1/2}\ . \tag{12}$$

The moments were calculated by Simpson's rule from the MEP fits (not from the raw data), treating n as a continuous variable, with suitable cutoffs at high and low n where $P(n)$ falls to $\epsilon=0.2$ times its peak. The lower cutoffs fell between $n=15$ and 27 and the upper cutoffs between 36 and 81 depending on the specific case. The overall pattern of variations of the means and ratios is not particularly sensitive to the choice of cutoff parameter ϵ.

The two ratios show a universal variation with reduced velocity (Figs. 10 and 11). In the new experiment [Fig. 10(a)], R_{KE} falls from 0.4 at $\bar{v}=0.3$ to 0.16 at $\bar{v}=0.7$ but then appears to remain constant up to $\bar{v}=1.5$. R_{Bohr} [Fig.11(a)] falls from near 1.0 at $\bar{v}=0.3$ to 0.6 at $\bar{v}=1.0$ and then falls very gradually to 0.5 at $\bar{v}=1.5$ R_{Bohr} and R_{KE} are nearly independent of nl at a given $\bar{v}$ and are generally higher for d states than for s states. The reanalysis of the 1982 data yields similar results and shows that the behavior of the two ratios persists up to $\bar{v}=1.95$ and is consistent between equal-velocity Na^+ and Ar^+ projectiles. The narrowing of the final-state distribution at $\bar{v}=0.8$ is particularly striking for the case $Ar^+ + Na(25s)$ [Fig. 9(c)].

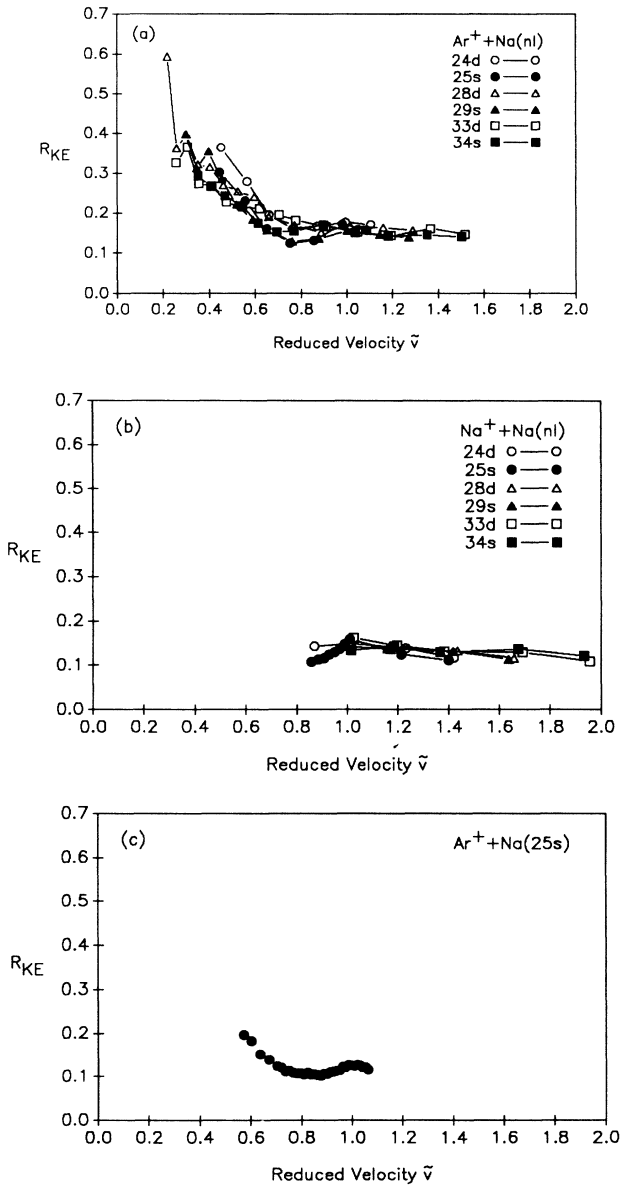

FIG. 10. Kinetic-energy spread ratio R_{KE}, Eqs. (7) and (11). (a) New $Ar^+ + Na(nl)$ data; (c) $Na^+ + Na(nl)$, 1982; (c) $Ar^+ + Na(25s)$ only, 1982.

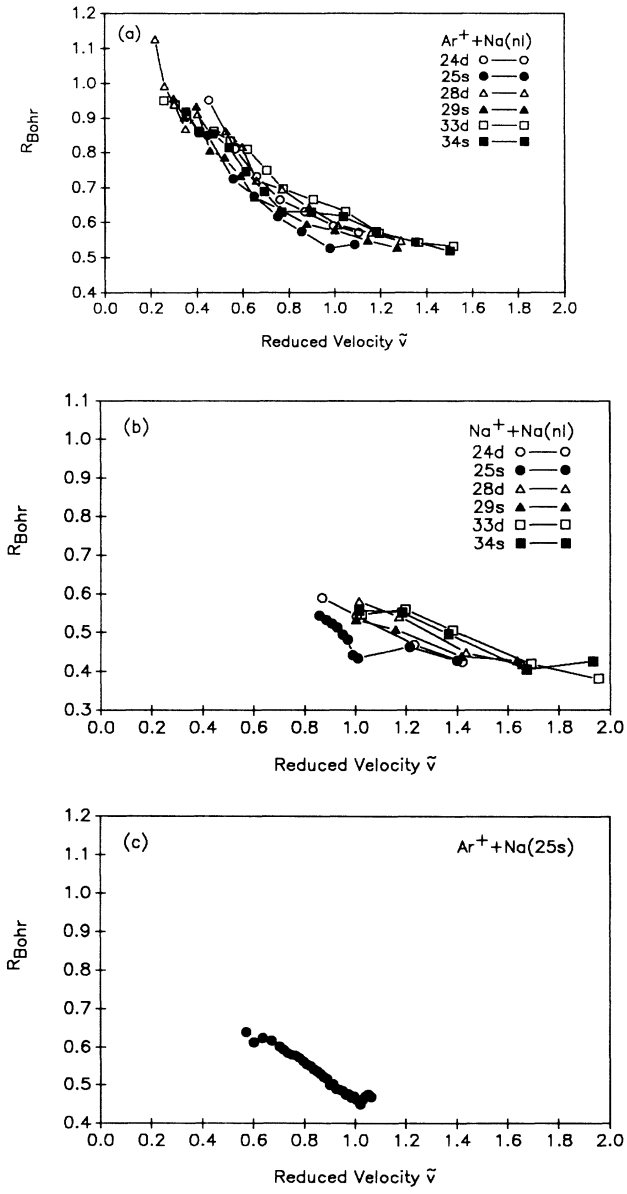

FIG. 11. Bohr-velocity spread ratio R_{Bohr}, Eqs. (10) and (12). (a) New $Ar^+ + Na(nl)$ data; (b) $Na^+ + Na(nl)$, 1982; (c) $Ar^+ + Na(25s)$ only, 1982.

The Oppenheimer-Brinkman-Kramers (OBK) approximation makes a simple prediction of the final-n distribution when averaged over initlal (l,m), summed over final angular momenta, and integrated over momentum transfer or scattering angle. As given by McDowell and Coleman,[45] the shell-to-shell OBK result (in a.u.) is

$$P^{\mathrm{OBK}}(n)=\frac{2^8\pi(Z_1Z_2)^5}{5v^2n_i^5n^3\beta^5} \tag{13}$$

where

$$\beta=(4v^2)^{-1}[v^4+2v^2(Z_2^2/n_i^2+Z_1^2/n^2) +(Z_2^2/n_i^2-Z_1^2/n^2)^2] . \tag{14}$$

Here, Z_1 and Z_2 are projectile and target-core charge numbers, respectively (both equal to one for the present work). v is the projectile velocity (a.u.) relative to the target, so that $\bar{v}=n_{\mathrm{eff}}v$. The OBK approximation is applicable to velocities $\bar{v}>1$.

In order to compare OBK with the experimental results and MEP parametrization, (13) was calculated for $\bar{v}=0.5$ to 2.0 and $n_i=24$, 28, and 33. These OBK distributions were fitted by the MEP between $n=21$ and 49 as for the centroid fits of experimental data. The resulting n_{max} and μ curves are shown in Figs. 8(d) and 9(d), respectively.

VI. CONCLUSION

Electrons are captured from state-selected Rydberg target atoms into a distribution of Rydberg states of the intermediate-velocity projectile. A wide spectrum of projectile bound states is populated, about 20 or more n values, and the angular momenta l and m in each n shell are not concentrated in a narrow range of values. The shape of the n distribution varies with projectile velocity and exhibits small differences between Na s-state targets and l-mixed targets, $l\geq 2$. l change of a target atom may occur during the approach of the capturing ion in addition to l mixing that occurs in the state-selected target prior to electron capture because of the more distant passage of other ions. If capture occurs at a well-defined internuclear separation, then rotation of the internuclear axis subsequent to capture causes a transformation and mixing of m sublevels to the extent of the electronic wave function's inability to adjust adiabatically to the rotation. Over the projectile velocity range of this study the rate of rotation for impact parameters comparable to the orbital radius varies from 0.2 to 2.0 times the characteristic orbital frequency. Thus rotational mixing may represent an intermediate case between adiabatic and diabatic behavior with regard to $\Delta n=\pm 1$ changes but is rapid with regard to mixing within a given n shell. Following capture, and after most of the axis rotation is complete, the wave functions centered on the receding projectile are still strongly perturbed by the Coulomb field of the residual target core. The final distribution of l and m is governed by the way that the corresponding Stark levels relax into projectile angular momentum states.

Two relative measures have been defined, R_{KE} and R_{Bohr}, to describe the evolution of electronic motion in the electron-capture process. Both measures demonstrate that the dynamics of the three-charged-particle encounter impose a $\bar{v}$-dependent electronic-velocity or kinetic-energy spread that is approximately fixed for $\bar{v}>1$ in relation to the initial velocity or kinetic energy. However, the spreads broaden in a nearly universal way among target states in slower collisions. Even in the absence of more detailed experimental or theoretical insight into the nature of the final-state distributions and their velocity dependence, these characteristics of the Rydberg capture process beg for interpretation.

The OBK approximation, given its severe shortcomings both at $\bar{v}=1$ and at asymptotically high velocities,[45,46] gives a familiar and easily calculated standard against which the present experimental results may be compared. Its prediction of relative distributions is known to be much better than its measure of the absolute cross section.[45] OBK predict final-state distributions centered near n_i and shifting with $\bar{v}$ in a manner roughly similar to the experimental data, but the OBK shift is much more gradual. The sharpness of distributions (indicated by μ) is poorly represented by OBK, which indicates considerably broader distributions and shows no sharpness maximum at an intermediate velocity.

The problem of electron capture at $\bar{v}\approx 1$ from a Rydberg target into Rydberg states presents a distinctly quantum-mechanical problem in a high-quantum-number limit. Many hundreds of atomic states are strongly coupled, and the interferences, tunneling, and the discreteness of stationary states are all essential to the behavior of the system. The broad spectrum of energy states near the initial state, centered both on the target and on the projectile, the profusion of angular momenta or Keplerian orbital eccentricities, and the presence of isoenergetic continuum states allow this three-body system to respond virtually without restriction to the transient forces of the encounter. None of the currently discussed methods of collision theory seems capable of encompassing these features at intermediate velocity without becoming computationally intractable or numerically unstable. The need for prodigiously large basis sets, whether of atomic or molecular orbitals, itself shows that a coupled-channel approach may not be the right one.[47] We feel sure that the method suited to a detailed analysis of this problem has not yet been presented and that when it is it will find broad application in the quantum mechanics of strongly coupled time-dependent systems.

ACKNOWLEDGMENTS

We would like to thank Dr. Hong-de Luo and Xiaoyu Sun for performing the calculations of uniform-manifold DSFI signals. We thank J. F. McCann and J. D. Garcia for insights into the theory. Thanks also go to W. L. Fuqua III for generous electronics support. This work was supported in part by National Science Foundation Grants No. PHY-8507532 and No. PHY-8808022.

*Permanent address: Department of Physics, Transylvania University, Lexington, KY 40507.

[1]K. B. MacAdam, L. G. Gray, and R. G. Rolfes, in *Abstracts of Contributed Papers, XVI International Conference on the Physics of Electronic and Atomic Collisions,* edited by A. Dalgarno *et al.,* (Elsevier, New York, 1989), p. 728.

[2]R. G. Rolfes and K. B. MacAdam, J. Phys. B **15**, 4591 (1982).

[3]K. B. MacAdam and R. G. Rolfes, J. Phys. B **16**, 3251 (1983).

[4]K. B. MacAdam, in *Electronic and Atomic Collisions,* edited by J. Eichler, I. V. Hertel, and N. Stolterfoht (Elsevier, Amsterdam, 1984), p. 265.

[5]J. S. Briggs, in *Semiclassical Description of Atomic and Nuclear Collisions,* edited by J. Bang and J. De Boer (Elsevier, Amsterdam, 1985), p. 183.

[6]R. G. Rolfes, D. B. Smith, and K. B. MacAdam, Phys. Rev. A **27**, 2378 (1988).

[7]K. B. MacAdam, R. G. Rolfes, and D. A. Crosby, Phys. Rev. A **24**, 1286 (1981); D. B. Smith, Ph.D. dissertation, University of Kentucky, 1987 (unpublished).

[8]K. B. MacAdam, D. B. Smith, and R. G. Rolfes, J. Phys. B **18**, 441 (1985).

[9]C. Harel, and A. Salin, J. Phys. B **10**, 3511 (1977). The authors discuss a variation of binding energy of the captured electron that is similar to the behavior observed here in the same range of scaled velocity.

[10]A. Salin, J. Phys. (Paris) **45**, 671 (1984).

[11]C. Harel and A. Salin, in *Electronic and Atomic Collisions,* edited by H. B. Gilbody *et al.* (Elsevier, Amsterdam, 1988), p. 631.

[12]R. K. Janev and H. Winter, Phys. Rep. **117**, 265 (1985).

[13]R. E. Olson, Phys. Rev. A **24**, 1726 (1981).

[14]T. P. Grozdanov and R. K. Janev, Phys. Rev. A **17**, 880 (1978).

[15]C. Harel and H. Jouin, J. Phys. B **21**, 859 (1988).

[16]T. P. Grozdanov and D. C. Belic, Phys. Scr. **30**, 194 (1984).

[17]J. Burgdörfer, Nucl. Instrum. Methods A **240**, 519 (1985); J. Burgdörfer and L. Dubé, Phys. Rev. A **31**, 634 (1985).

[18]J. Burgdörfer, R. Morgenstern, and A. Niehaus, J. Phys. B **19**, L507 (1986).

[19]A. Jain, C. D. Lin, and W. Fritsch, J. Phys. B **21**, 1545 (1988).

[20]R. E. Olson, J. Phys. B **13**, 483 (1980); R. C. Isler and R. E. Olson, Phys. Rev. A **37**, 3399 (1988).

[21]R. L. Becker and A. D. MacKellar, J. Phys. B **17**, 3923 (1984).

[22]A. D. MacKellar and R. L. Becker, in *Abstracts of Contributed Papers, XIII International Conference on the Physics of Electronic and Atomic Collisions,* edited by J. Eichler *et al.* (Elsevier, New York, 1983), p. 660.

[23]M. C. Brower and F. M. Pipkin, Phys. Rev. A **39**, 3323 (1989).

[24]J. R. Ashburn *et al.,* Phys. Rev. A **41**, 2407 (1990).

[25]D. Vernhet *et al.,* J. Phys. B **21**, 3949 (1988).

[26]A. Müller *et al.,* Phys. Rev. A **36**, 599 (1987).

[27]B. D. DePaola *et al.,* Nucl. Instrum. Methods B **40/41**, 187 (1989).

[28]K. B. MacAdam and R. G. Rolfes, Rev. Sci. Instrum. **53**, 592 (1982).

[29]K. B. MacAdam and R. G. Rolfes, J. Phys. B **15**, L243 (1982).

[30]T. Åberg, A. Blomberg, and K. B. MacAdam, J. Phys. B **20**, 4795 (1987).

[31]C. E. Theodosiou, Phys. Rev. A **30**, 2881 (1984). The calculated Na lifetimes including blackbody radiation at 410 K were used.

[32]T. H. Jeys *et al.,* Phys. Rev. Lett. **44**, 390 (1980).

[33]*Rydberg States of Atoms and Molecules,* edited by R. F. Stebbings and F. B. Dunning (Cambridge University Press, New York, 1983).

[34]M. G. Littman, M. L. Zimmerman, and D. Kleppner, Phys. Rev. Lett. **37**, 486 (1976).

[35]T. F. Gallagher *et al.,* Phys. Rev. A **16**, 1098 (1977).

[36]M. L. Zimmerman *et al.,* Phys. Rev. A **20**, 2251 (1979); D. A. Harmin, *ibid.* **26**, 2656 (1982); I. V. Komarov, T. P. Grozdanov, and R. K. Janev, J. Phys. B **13**, L573 (1980).

[37]K. B. MacAdam, R. G. Rolfes, X. Sun, J. Singh, W. L. Fuqua III, and D. B. Smith, Phys. Rev. A **36**, 4254 (1987).

[38]T. H. Jeys *et al.,* Phys. Rev. A **26**, 335 (1982).

[39]The conclusions of this study are insensitive to the choice between $f(n)=n$ and n^2 although the actual fitted MEP parameter values vary systematically with this choice.

[40]P. R. Bevington, *Data Reduction and Error Analysis for the Physical Sciences* (McGraw-Hill, New York, 1969).

[41]F. G. Kellert *et al.,* Phys. Rev. A **23**, 1127 (1981).

[42]R. J. Damburg and V. V. Kolosov, J. Phys. B **12**, 2637 (1979), Eq. (6).

[43]N. Hoe, B. D'Etat, and G. Coulaud, Phys. Lett. **85A**, 327 (1981).

[44]Note that in Ref. 30 the corresponding means were calculated with n_{eff} set equal to the integer n_l.

[45]M. R. C. McDowell and J. P. Coleman, *Introduction to the Theory of Ion-Atom Collisions* (North-Holland, Amsterdam, 1970).

[46]L. J. Dubé and J. S. Briggs, J. Phys. B **14**, 4595 (1981).

[47]M. Inokuti (private communication).